

Transmission of radio-frequency waves and nuclear magnetic resonance in lanthanum superhydrides

Dmitrii V. Semenok^{1,†,*}, Florian Bärtl^{2,3,†}, Di Zhou^{1,†,*}, Toni Helm^{2,4}, Sven Luther², Hannes Kühne², J. Wosnitza^{2,3}, Ivan A. Troyan⁵, and Viktor V. Struzhkin^{6,*}

¹ *Center for High Pressure Science and Technology Advanced Research (HPSTAR), Beijing*

² *Dresden High Magnetic Field Laboratory (HLD-EMFL) and Würzburg-Dresden Cluster of Excellence ct.qmat, Helmholtz-Zentrum Dresden-Rossendorf, 01328 Dresden, Germany*

³ *Institute for Solid State and Materials Physics, Technische Universität Dresden, 01062 Dresden, Germany*

⁴ *Max Planck Institute for Chemical Physics of Solids, 01187 Dresden, Germany*

⁵ *A.V. Shubnikov Institute of Crystallography of the Kurchatov Complex of Crystallography and Photonics (KMKiF), 59 Leninsky Prospekt, Moscow 119333, Russia*

⁶ *Shanghai Key Laboratory of Material Frontiers Research in Extreme Environments (MFree), Shanghai Advanced Research in Physical Sciences (SHARPS), Pudong, Shanghai 201203, China*

*Corresponding authors, emails: dmitrii.semenok@hpstar.ac.cn (Dmitrii V. Semenok), di.zhou@hpstar.ac.cn (Di Zhou), viktor.struzhkin@hpstar.ac.cn (Viktor V. Struzhkin).

†These authors contributed equally to this work

Abstract

The discovery of near-room temperature superconductivity in the lanthanum hydride LaH₁₀ has revolutionized this field of research. Until recently, the need to use diamond anvils for the synthesis of polyhydrides severely limited the list of experimental techniques that could be used to study these materials. Nuclear magnetic resonance (NMR) is one of the key methods for probing spin systems of superconductors. In this work, we show how ¹H NMR measurements can be realized in diamond anvil cells to study high-temperature superconductivity in lanthanum polyhydrides at pressures up to 165 GPa. We observed a pronounced suppression of the ¹H NMR signal intensity below $T_c^{\text{onset}} = 260$ K in a magnetic field of 7 T, corresponding to the screening of the radio-frequency pulses by the newly discovered superhydride LaH₁₂. Below the critical temperature of superconductivity, all ¹H NMR characteristics, including the spin-lattice relaxation rate $1/T_1T$, demonstrate pronounced features, indicating a superconducting transition in the sample. In the absence of an applied magnetic field, the radio-frequency signal transmission through the LaH₁₂ sample shows a pronounced drop below $T_c^{\text{onset}} \approx 267$ K, confirming the superconducting nature of the transition. Fitting the nuclear spin-lattice relaxation data allows the estimation of the superconducting gap $\Delta(0)$ between 427 and 671 K (corresponding to 36.8 to 57.8 meV), and the ratio $R_\Delta = 2\Delta(0)/k_B T_c$ between 3.76 and 5.16 in the synthesized hydride sample.

Keywords: NMR, superhydrides, superconductivity, radio-frequency methods, high-pressure.

Introduction

Superhydrides are a rapidly developing class of hydrogen-enriched compounds that have attracted considerable attention in the field of condensed matter physics due to their remarkable superconducting properties. The discovery of high-temperature superconductivity in H₃S ($T_c^{\text{max}} = 203$ K¹), LaH₁₀ ($T_c^{\text{max}} = 250$ K^{2,3}), ThH₁₀ ($T_c^{\text{max}} = 161$ K⁴), YH₆ ($T_c^{\text{max}} = 224\text{-}226$ K^{5,6}), CeH₁₀ ($T_c^{\text{max}} =$

115 K⁷) and many other polyhydrides^{8,9}, has opened new avenues for fundamental and applied studies. Particularly, the search for room-temperature superconductors and the development of magnetic field sensors, diodes, and memory elements based on superhydrides gave a new impetus to the research efforts¹⁰⁻¹². Unfortunately, polyhydride samples are often inhomogeneous^{13,14}. A comprehensive study of superconductivity (SC) in such inhomogeneous samples is problematic due to the presence of several crystallographic phases, including metastable ones¹⁵, with very different T_c 's (Figure 1a). Indeed, impurity hydride phases or grains, separated from the current trajectories by non-superconducting lower hydrides or insulating shells of higher polyhydrides, cannot be identified by standard four-probe transport measurements (Figure 1a). Such grains with varying superconducting properties may be responsible for broadened or steplike transitions in the temperature dependence of the resistance, hardly distinguishable inhomogeneous sample quality, or stress distributions. Detection methods based on volume-penetrating electromagnetic fields may be suitable probes in this situation. Radio-frequency (RF) contactless measurements^{16,17} or nuclear magnetic resonance (NMR) spectroscopy^{18,19} allow to overcome this problem and detect superconductivity in inhomogeneous samples under pressure.

NMR spectroscopy is based on the coherent manipulation of the nuclear spin system in a material containing nuclei with non-zero nuclear moment^{20,21}. NMR can be employed to probe the hyperfine magnetic fields, originating from the electronic subsystem. Thus, it is very sensitive to the static electronic spin susceptibility and low-energy excitations of the electronic system. The shape of an NMR spectrum, its broadening and frequency shift depend on the magnetic interactions of the nucleus with its environment²². ²⁷Al NMR spectroscopy played a major role in confirming the Bardeen–Cooper–Schrieffer (BCS) theory of superconductivity²³. Moreover, Redfield, Anderson, Hebel and Slichter discovered that at temperatures below the critical temperature (T_c), there is a minimum of the spin-lattice relaxation time T_1 (the Hebel-Slichter peak) in aluminum²⁴⁻²⁶. Measurements of T_1 at temperatures well below T_c yield an exponential increase of T_1 in the case of an isotropic superconducting gap. In metals, the NMR frequency shift (also called Knight shift²⁷) and the spin-spin relaxation time T_2 are independent of temperature²⁸, whereas $1/T_1$ is proportional to the temperature (known as Korringa relation²⁹). A distinctive feature of a superconducting transition is a sharp decrease of the relaxation rate $1/T_1T$ due to the opening of the superconducting gap.

From the beginning of research on superhydrides, it was suggested they were the most prominent representatives of BCS superconductors¹. NMR spectroscopy is a powerful tool for studying the nature of the normal and superconducting groundstate. Therefore, it can help to obtain information on the superconducting gap in the polyhydrides. To date, the challenge was the need to create enormous pressures above 1 million atmospheres (100 GPa) in a tiny sample volume of a diamond anvil cell's (DACs) chamber. Here, the comparably high sensitivity of NMR spectroscopy to the ¹H isotope, the sublattice of which plays a major role in the superconductivity of hydrides⁸, is very beneficial. Fortunately, an approach has recently been developed that allows the detection of ultra-small samples via conventional solid-state NMR techniques, using focusing Lenz lenses deposited on diamond anvils^{18,30,31}. Lower hydrides of iron FeH³², copper Cu₂H³³, yttrium YH₃¹⁸, LaH₃³¹, and molecular hydrogen^{34,35}, have previously been studied at pressures up to 220 GPa. Below, we will demonstrate that the same Lenz lenses prove to be a very efficient tool for studying the surface impedance of superhydride samples. Unlike NMR, within this RF method, two Lenz lenses are used separately as excitation (A) and detection (B) microcoils of an RF transformer (Figure 1a).

In this work, we applied radio-frequency transmission and proton NMR techniques to the study of lanthanum superhydrides, synthesized from La or LaH₃ and ammonia borane (NH₃BH₃, AB) in five DACs (labeled as “N0-N4”) at different pressures up to 165 GPa. We were able to study the ¹H NMR signal of various lanthanum polyhydrides and observed the superconducting transition stemming from the newly discovered (pseudo)hexagonal LaH₁₂, yielding a T_c^{onset} of at least 267 K.

This is confirmed by an abrupt change in the RF surface impedance and a sharp drop of the ^1H NMR spin-lattice relaxation rate.

Results and discussion

1. Combined DAC with electrodes and Lenz lens

Although the radio-frequency method of measuring surface impedance has been known since 1989¹⁶, and has been widely used to detect superconducting transitions^{17,36}, it has not been applied in combination with Lenz lenses³⁷ for high-pressure studies. To bridge this gap, in the first (calibration) experiment with DAC N0 (Figure 1a-e), we used two detection systems simultaneously: a classical four-probe van der Pauw resistance measurement circuit was deposited on one diamond anvil, while a simple single-stage Ta/Au Lenz lens (Figure 1b) was sputtered onto the opposite anvil. After laser heating of La microparticles loaded with ammonia borane (NH_3BH_3) at 149 GPa, the pressure in the DAC dropped to 120 GPa, and the four-contact electrical measurements showed a pronounced drop of the sample's resistance starting below $T_c^{\text{onset}} = 205$ K (Figure 1d). This critical temperature is in good agreement with previous decompression studies of the La superhydride³⁸. The result of our synthesis may correspond to the polyhydride LaH_{9+x} ($x = -1 \dots +1$) with a low symmetry (e.g., $C2/m$ ³⁸), and, partially, a molecular hydrogen sublattice³⁹. A detailed description of the preparation and characteristics of DAC N0 is given in the Supporting Table S1.

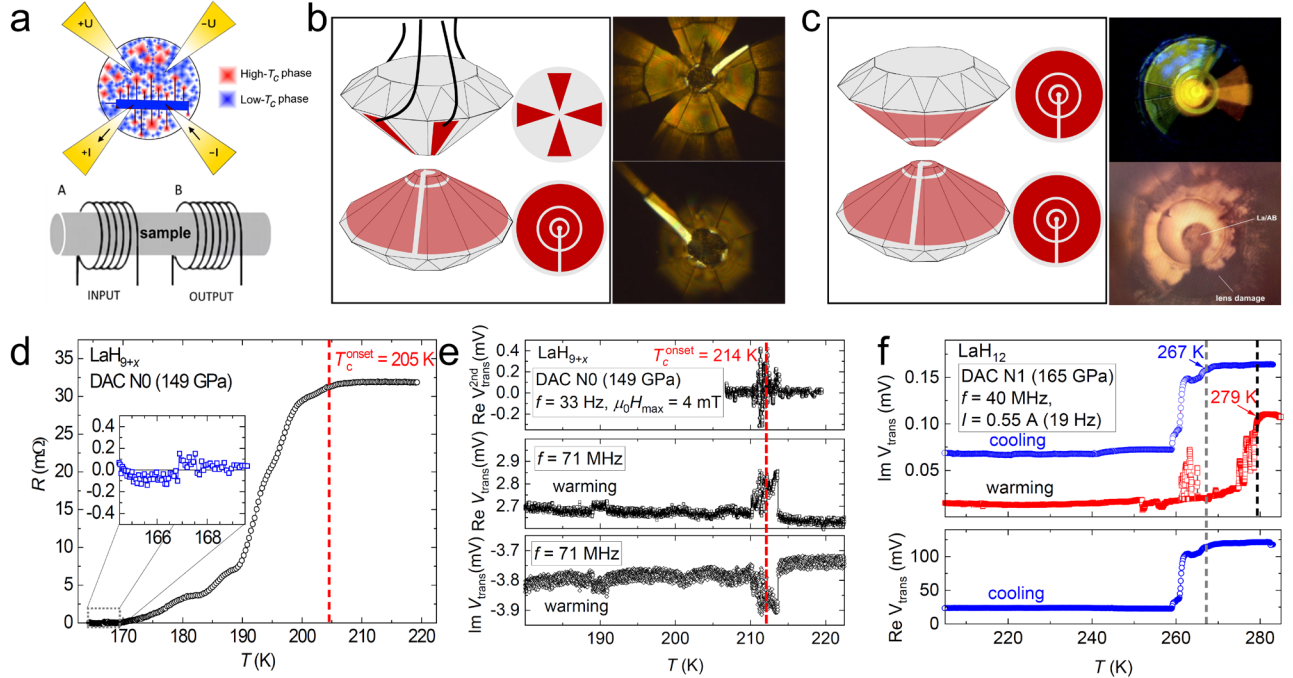


Figure 1. Electrical resistance and RF transmission response of lanthanum superhydrides, synthesized from La and NH_3BH_3 in DACs N0 and N1. (a) A sketch of a possible distribution of high- T_c and low- T_c superconducting phases in a hydride sample, which complicates the detection of high- T_c superconductivity using a 4-electrode van der Pauw circuit. At the same time, the low- T_c transition can be detected due to the presence of a homogeneous segment of the corresponding phase (marked in blue) between the current electrodes. Also shown is the scheme of RF diagnostics of sample properties employing a transformer circuit (coil A is input, coil B is output). (b) Schematic diagram of the DAC N0, containing a 4-electrode circuit for transport measurements and a Lenz lens for RF transmission measurements. Photographs of the DAC's culet, loaded sample, electrode system (1-4) and Lenz lens. (c) Schematic diagram of the DAC N1, containing two Lenz lenses for RF transmission measurements and NMR. Photographs of the anvil culet with sputtered Lenz lenses of DAC N1 before and after loading and compression to 165 GPa. (d) Electrical resistance (current is 1 mA, DC) as a function of temperature for a sample of lanthanum hydride in DAC N0 at 120 GPa. Inset: residual resistance of the sample below 170 K. (e) Real (Re) and imaginary (Im) components of the RF signal passing through the DAC N0 sample in transformer mode. The carrier frequency is 71 MHz. Top panel: directly demodulated RF signal on the 2nd harmonic of the low-frequency modulating field (33 Hz, $B_{\text{max}} \approx 4$ mT). (f)

High-frequency (40 MHz) study of the DAC N1 at 165 GPa. Real and imaginary components of the receiving coil signal in the cooling cycle. The superconducting transition in DAC N1 starts around 267 K. Thermal hysteresis (about 10 to 12 K) in the system as exemplified by the imaginary (Im) components of the receiving coil signal. Thermometer was glued to the outside of the DAC N1.

Using any pair of electrodes of the DAC N0 as a radio-frequency antenna and the Lenz lens with a surrounding, macroscopic single-turn coil as a receiver (Supporting Figures S1, S2) allows us to detect a sharp change in the surface impedance of the sample in the real and imaginary components of the RF signal. It corresponds to the SC transition, with an onset already at 212 to 214 K (Figure 1e). We detected the step or jump of the transmitted RF signal with various frequencies, such as 1, 4, 20 and 71 MHz (Figure 1e, Supporting Figure S4) confirming its reproducibility. For additional verification, we used the double-modulation technique, similar to that proposed by Timofeev in 2002¹⁷. As shown in the inset of Figure 1e, placing the sample in a weak ($B_{max} \approx 4$ mT) oscillating magnetic field with a frequency of 33 Hz leads to a pronounced feature in the 2nd harmonic (66 Hz) of the directly demodulated RF signal. It emerges simultaneously with the jump in the transmitted RF signal, because the magnetic field suppresses superconductivity, regardless of the direction of the magnetic induction vector \vec{B} .

The critical temperature observed for DAC N0 by the RF method is somewhat higher than T_c^{onset} , detected by means of the resistive measurements. This is because the high-frequency field penetrates the entire volume occupied by the LaH_{9+x} sample, and not only the interelectrode space, as in the case of 4-electrode circuit. That is why it is possible to detect superconducting phases with the highest T_c 's regardless of how far they are from the electrodes. Note that reducing the carrier frequency to 100 to 500 kHz also allows for reliable detection of the signal of only the "main" superconducting phases, located near the electrodes, with T_c at about 180 to 190 K (Supporting Figure S4).

2. Radio-frequency detection of superconductivity with two Lenz lenses

After successful testing of the RF contactless detection method with Lenz lenses on the example of LaH_{9+x} (DAC N0), we prepared samples containing two three-stage Lenz lenses for combined RF transmission and ¹H NMR studies. We performed experiments with four different high-pressure diamond anvil cells (pressure is given in brackets): DAC N1 (165 GPa), N2 (147 GPa), N3 (87 GPa), and N4 (19 GPa). The samples in the DACs N1 and N2 were obtained by infrared laser heating of metallic La in an NH₃BH₃ environment, while the samples N3 and N4 were obtained by heating of LaH_{~3} with NH₃BH₃ under pressure. The laser heating was carried out at the ID27 station of the European synchrotron radiation facility (ESRF). The most interesting results were obtained for the samples N1 and N3, synthesized in symmetric BX-90 mini cells⁴⁰, equipped with diamond anvils with a culet diameter of 75 μm . Copper or silver films, sputtered onto diamond anvils with a thickness of 1-2 μm were used to make the Lenz lenses³⁷ (Figure 1c, Supporting Figures S1, S2). As we will demonstrate in the next paragraph, the sample in DAC N1 can be described by the formula LaH₁₂, which we will use in what follows. Detailed information on the DACs' design and preparation is given in the Supporting Table S1.

First, we performed RF transmission measurements of DAC N1 at 165 GPa, employing a high-frequency transformer formed by the two Lenz lenses. As can be seen in Figure 1f, the RF signal transmission in DAC N1 exhibits a main feature at 267 to 286 K, which shows up in both the amplitude and phase of the output signal of the RF transformer for various frequencies (40, 150, and 200 MHz). It is accompanied by the appearance of a second harmonic at the frequency of the external modulation field (Supporting Figure S5). A rather small feature in the RF transmission behavior of the sample is also observed at 248 to 252 K, which probably corresponds to the LaH₁₀ impurity (Supporting Figure S6). Previous works on lanthanum^{3,41-43} and lanthanum-scandium¹² hydrides indeed reported an additional step-like drop in the electrical resistance setting in at temperatures between 265 and 280 K or even above. However, such a high T_c could not be attributed to any known

La hydride until now. In the present work, we demonstrate that this high- T_c hydride phase can be detected by contactless methods, in particular by changes in the surface RF impedance. The RF method reported here, indicates that superconductivity in the La-H system under pressure may occur already at temperatures as high as 267 to 286 K^{12,42}.

3. X-ray diffraction of the synthesized lanthanum superhydrides

Diffraction of synchrotron radiation is effective in elucidating the structure of polyhydrides under high pressure. The structures of the lanthanum superhydrides obtained in the DACs N1, N2 and N3 were studied using powder X-ray diffraction (XRD, Figure 2). In the case of the DAC N1, our X-ray diffraction analysis shows the formation of a new crystal modification of LaH_{12} at 165 GPa, most likely with a hexagonal $P6$ symmetry (Figure 2a). In general, an interpretation of the XRD data of the sample in DAC N1 at 165 GPa is challenging. The resulting pattern differs from all the previously experimentally studied ones for the La-H system. In terms of volume, the obtained compound approaches the one of LaH_{12} ².

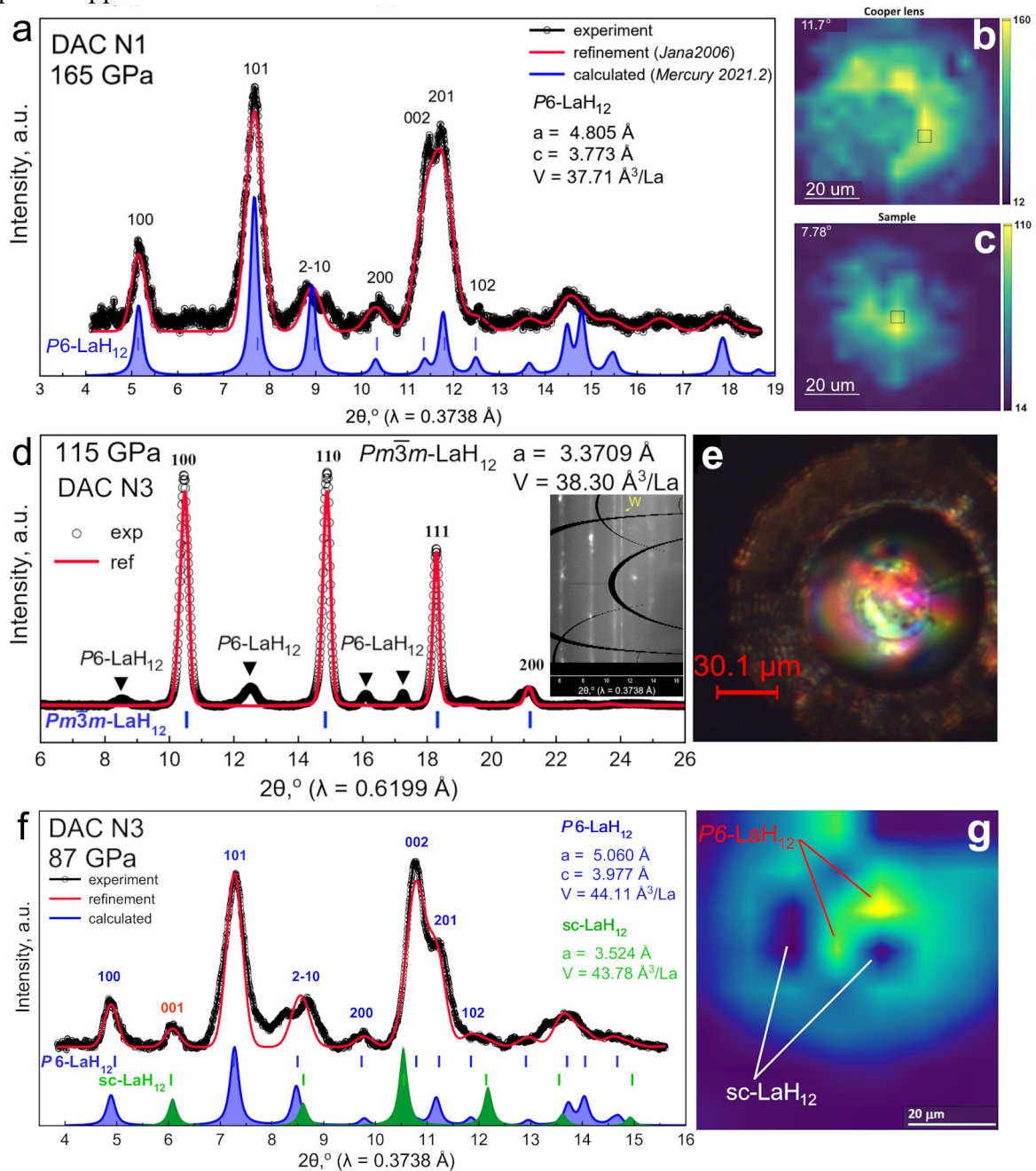


Figure 2. X-ray diffraction studies of the samples DAC N1 at 165 GPa and DAC N3 at 87-115 GPa. (a) X-ray diffraction pattern of the sample DAC N1 and Le Bail refinement of the $P6\text{-LaH}_{12}$ unit cell parameters. Black circles are the experimental data, the red line is the Le Bail refinement, and the blue line is the XRD

pattern calculated using the Mercury 2021.2 software⁴⁴. For the refinement, we used the $P6_3/mmc$ -LaH₉ structure, which explains almost all diffraction peaks, but has an unusual c/a ratio of 0.77. The unit cell volume corresponds to a hydrogen content of ≈ 12 H atoms per La atom. (b) X-ray diffraction mapping of a copper Lenz lens, and (c) the $P6$ -LaH₁₂ distribution, XDI software⁴⁵. (d) X-ray diffraction pattern of the sample in DAC N3 and Le Bail refinement of the $Pm\bar{3}m$ -LaH₁₂ unit cell parameters. The sample also contains an impurity fraction of hexagonal $P6$ -LaH₁₂. Black circles are the experimental data, the red line is the Le Bail refinement. (e) Photograph of DAC's N3 culet with the sample. (f) XRD pattern of the sample in DAC N3 after decompression to 87 GPa. Black circles are the experimental data, the red line is the Le Bail refinement, and the blue and green filled curves are the XRD patterns of both LaH₁₂ modifications, calculated using the Mercury 2021.2 software⁴⁴. (g) X-ray diffraction map of the $P6$ - (yellow-green) and $Pm\bar{3}m$ -LaH₁₂ (dark blue) spatial distributions (XDI software⁴⁵).

Although the $P6_3/mmc$ structure, with the lattice parameters $a = 4.805 \text{ \AA}$ and $c = 3.773 \text{ \AA}$, and a unit cell volume of $V = 37.71 \text{ \AA}^3/\text{La}$, describes the observed diffraction pattern quite well (Figures 2a-c), it should be noted that a c/a ratio of 0.78 is unusually small for the $P6_3/mmc$ space group. Moreover, the reflections 002 and 201 have unexpectedly high intensities. Hence, another (lower) space group may also describe the structure of the obtained compound. The amount of hydrogen in the $P6$ -LaH₁₂ is established by analogy with the previously reported simple cubic (sc) $Pm\bar{3}m$ -LaH₁₂^{2,46-48} with an accuracy of ± 1 H atom.

The sample in DAC N3, consisting of two phases, was initially synthesized at a pressure of about 115 GPa from LaH₋₃ and ammonia borane (NH₃BH₃). The first phase detected after the pressure synthesis (115 GPa) was simple cubic ($Pm\bar{3}m$) sc-LaH₁₂ (Figure 2d-e), as reported previously^{2,46-48}. The second phase, distributed in close proximity to LaH₁₂, is the hexagonal modification $P6$ -LaH₁₂, which is the main product of the synthesis in DAC N1. This $P6$ phase has almost the same volume as the cubic one (Figure 2f-g). Both synthesized modifications of LaH₁₂ generally retain the structure of their La sublattices upon decompression to 87 GPa (Figure 2f).

DAC N2, made from BeCu alloy, was loaded with metallic La and NH₃BH₃, and heated via a series of IR laser pulses at 147 GPa at the ID27 station of the ESRF. After the laser heating, the pressure increases to 150 GPa. For this sample, we used diamond anvils with a culet diameter of 100 μm . As will be discussed below, the ¹H NMR signal of the sample in DAC N2 is several times lower as compared those of the ones in DACs N1 and N3. This likely is caused by the partial destruction of one of the Lenz lenses, and a comparably small amount of synthesized superhydrides.

According to the X-ray diffraction analysis (Supporting Figure S16), there are two small regions of $\sim 10 \mu\text{m}$, containing mainly $I4/mmm$ -LaH₄ and $Cmcm$ -LaH₃ in the sample space of DAC N2. The first of these compounds is a superconductor with a critical temperature of about 80 to 90 K^{49,50}, while the second one is an analogue of the previously found $Cmcm$ -LaH₋₄¹⁴ with an unit-cell volume less by $2 \text{ \AA}^3/\text{La}$. This corresponds to the LaH₃ composition. The T_c of the tetragonal LaH₄ was reported to decrease rapidly in an applied magnetic field ($dT_c/dB \approx -2 \text{ K/T}$ ⁴⁹). It may be estimated as approximately 66 to 76 K at 7 T. Due to the low content of the superconducting phase and the large spurious background signal with features below 100 K, we cannot confidently state that we have detected the anticipated superconducting transition in LaH₄. However, the disappearance of a series of ¹H NMR signals, and a step in the $1/T_1$ vs T dependence around 60 to 70 K may indicate the emergence of superconductivity in LaH₄ (Supporting Figure S27, S28).

DAC N4 was loaded with LaH₋₃ and NH₃BH₃. It was heated by an IR laser at around 150 GPa, but it broke down in the following days with a pressure drop below 50 GPa. Due to this, DAC N4 was used only for a narrow set of experiments (Supporting Figure S29).

4. Comparative NMR experiments

Proton NMR experiments on micron-sized samples compressed between diamond anvils are inevitably associated with large parasitic ¹H NMR signals from different parts of the high-pressure DACs, such as the organic adhesive used to glue diamond anvils to the seats, wire insulation, capacitors, soldering paste, or the printed circuit board (PCB) supporting the excitation coils. Since

the laser heating in DACs never leads to a complete decomposition of NH_3BH_3 , the study of the residual signal of this compound is important as well. Therefore, before starting the experiments with the polyhydrides in the DACs N1-N4, we investigated several calibration samples at temperatures from 10 to 300 K. We studied the following test samples:

- (A) An empty high-pressure DAC with a Lenz-lens system (Supporting Figure S7);
- (B) The same DAC loaded with a piece of ^{27}Al foil and NH_3BH_3 (Supporting Figures S8-S9);
- (C) A bulk sample of ammonia borane in a solenoid coil (Supporting Figures S10-S11);
- (D) A piece of PCB serving used as support for the excitation coils (Supporting Figure S12).

As a result of these preliminary experiments, we found that the Lenz-lens system does indeed allow a reliable detection of the ^{27}Al NMR signal from a small piece of Al foil (test sample B), although the spin-lattice relaxation curve $I(\tau)$ and the stretching exponent indicate a non-uniform distribution of the RF field in the sample (Supporting Figure S9). As we will discuss below, this also plays a role in the study of superhydride samples, increasing the inaccuracy of the T_1 determination.

The teflon PCB gives an insignificant ^1H NMR signal without pronounced features above 170 K (Supporting Figure S12). An examination of the empty DAC with Lenz lenses may indicate the presence of some volatile H-containing compounds that are entrained in a He flow: the NMR signal intensity significantly decreases with time (Supporting Figure S7). The low intensity of the reproducible NMR signal of the empty DAC does not allow the determination of a related T_1 . The ^1H signal intensity increased significantly when we placed a micron-sized sample of NH_3BH_3 together with the ^{27}Al foil test sample in the chamber of the empty test DAC (Supporting Figures S8, S9). Despite the presence of a kink in the temperature dependence of the integral intensity $I(T)$, the nuclear spin-lattice relaxation rate $1/T_1T$ yields no particular features between 50 and 300 K (Supporting Figure S8), which is important to note for the subsequent experiments on the lanthanum hydrides.

Finally, the ^1H NMR experiments on a bulk sample of NH_3BH_3 points to a rather complex, two-component relaxation behavior of this compound. For instance, the spin-lattice relaxation rate $1/T_1T$ yields a rise below 210 K, with a maximum at 100 to 150 K (Supporting Figures S10, S11). It is possibly related to low-temperature phase transitions in NH_3BH_3 , as reported previously (see also Ref.⁵¹).

4. ^1H NMR of the lanthanum superhydride at 165 GPa

A system of Lenz lenses (Figure 3a-b), deposited on diamond anvils, can be used to perform NMR measurements of micron-sized samples under pressure. Our ^1H NMR study of the DAC N1 in a magnetic field of 7 T ($\nu_0 = 298$ MHz), employing a conventional spin-echo pulse sequence, were carried out in a cooling cycle at temperatures from 300 to 10 K (Figure 3c). At high temperatures, the spectrum can be described as a composition of at least four peaks (Figure 3d, “a-d”), three of which (“a-c”) disappear below 230 K, yield a negative frequency shift with decreasing temperature ($d\nu/dT > 0$), and are attributed to different lanthanum superhydrides. These phases form at 165 GPa when the La/AB mixture is heated^{2,14,39}. As the X-ray diffraction analysis demonstrated (Figure 2), the main phase synthesized in DAC N1 is the hexagonal $P6$ -LaH₁₂. The very narrow peak “d” disappears below 200 K and yields $d\nu/dT < 0$. Between 300 K and $T_c^{\text{onset}} = 260$ K, we find a linear decrease of the integral intensity of the NMR spectrum, as well as a pronounced change in the slope at T_c^{onset} . Below T_c^{onset} , our data show a strong suppression of the NMR intensity, which saturates at $T_c^{\text{offset}} = 211$ K. Between T_c^{onset} and 220 K, we observe pronounced changes in all integral spectral characteristics, i.e., the amplitude, frequency shift, spectral width, and area of the ^1H NMR spectrum (Figure 3d, Supporting Figure S21). The residual, broad low-temperature ^1H NMR spectrum stems from the background of non-superconducting hydrogen-containing compounds, residual NH_3BH_3 , products of its thermal decomposition, and lower La hydrides. (Figures 3c,d). We note that, although

these background signals may partially contribute to the change in spectral characteristics in the superconducting transition region, this does not affect the qualitative behavior in the detection of the superconducting transition by means of NMR spectroscopy. At 165 GPa, the observed critical $T_c^{50\%}(7T)$ is 227 ± 5 K (Figure 1f). This temperature corresponds to the SC transition in the best-known lanthanum superhydrides in a field of 7 T, determined via electrical transport measurements at the middle of the resistance drop ($R_{50\%}$ criterion, see Ref. ²).

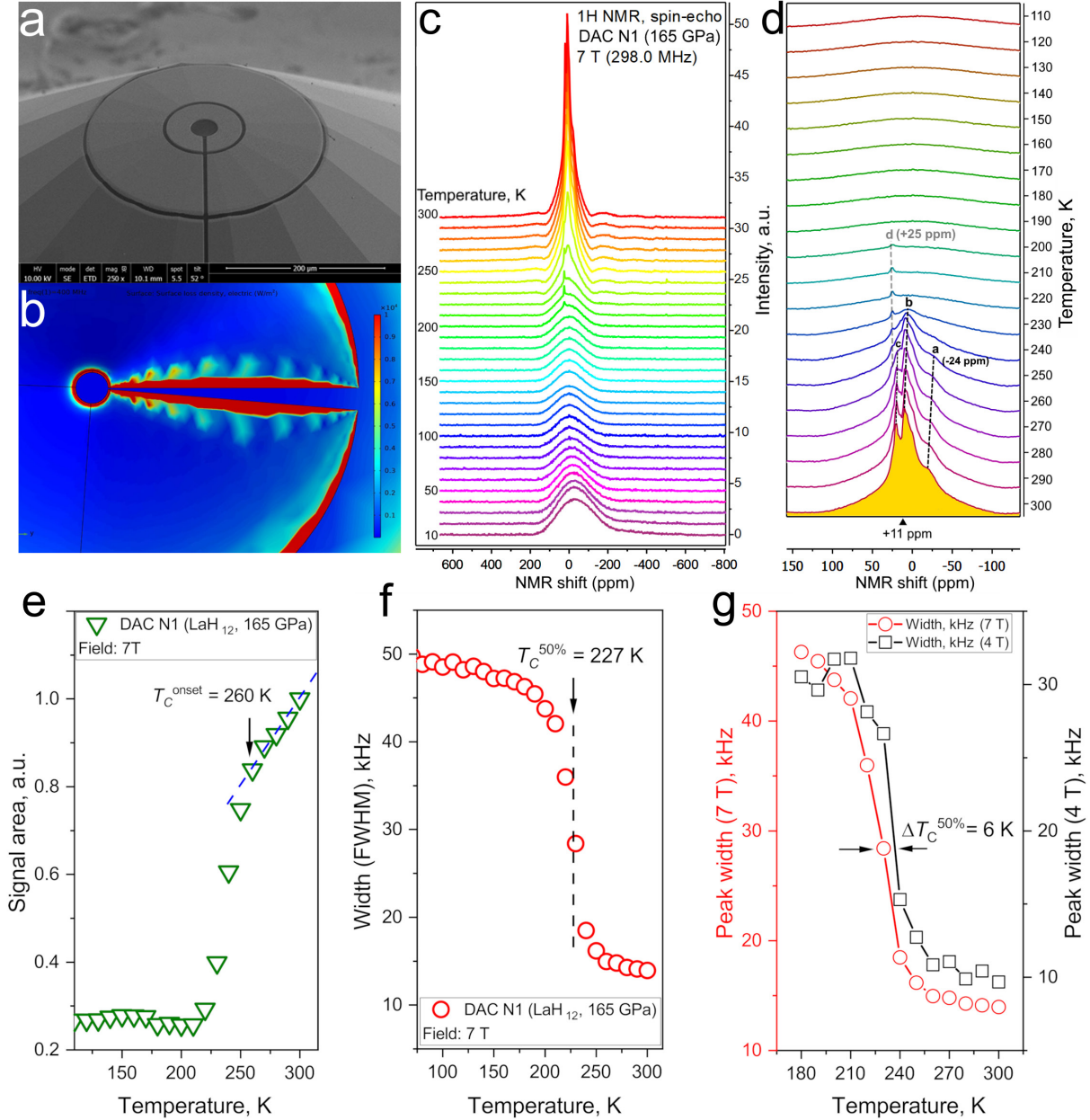


Figure 3. Nuclear magnetic resonance experiments using DAC N1. (a) Scanning electron microscopy of the copper Lenz lens of DAC N1, prepared by Ga focused ion beam. (b) Modeling of the distribution of surface current density losses (in W/m²) in the Lenz lens at 400 MHz (COMSOL Multiphysics ⁵²). (c) Stack of ^1H NMR spectra, recorded in a cooling cycle from 300 to 10 K in steps of 10 K. (d) ^1H NMR spectra in the temperature regime of the superconducting transition. The structure of the signal above 240 K is composed of at least four (“a-d”) different peaks. (e) Dependence of the ^1H NMR signal area (“intensity”) on temperature between 115 and 300 K. $T_c^{\text{onset}} = 260$ K denotes the onset of the pronounced decrease in the NMR signal intensity. (f) Dependence of the ^1H NMR linewidth (FWHM) on temperature between 75 and 300 K, yielding $T_c(50\%) = 227 \pm 5$ K. (g) Temperature dependence of the linewidth for applied magnetic fields of 4 and 7 T. At 4 T, T_c is approximately 6 K higher.

The expected superconducting transition in the lanthanum superhydride in DAC N1 in a lower field of 4 T is shifted higher in temperature, up to $T_c^{50\%} \approx 235 \pm 5$ K (Figure 3g). The offset critical temperature also increases with decreasing magnetic field: from 211 K (7 T) to 220 K (4 T), see

Supporting Figure S22. In general, the behavior of the NMR signal and the spin-lattice relaxation times of DACs N1 and N3 is very similar. This can be understood by the presence of the same $P6\text{-LaH}_{12}$ phase in both samples.

To confirm the onset of superconductivity as origin of the pronounced change in the spectral features of the DAC N1 sample, we also measured the nuclear spin-lattice relaxation time T_1 . The relaxation rate $1/T_1T$ in DACs N1 and N3 begins to decrease at temperatures above 260 K in a field of 7 T (Figure 4a). A sharp drop in $1/T_1T$ by 3-6 times relative to the calibration samples and other DACs in the same temperature range of 220 to 260 K indicates the superconducting nature of the transition in the lanthanum hydride samples N1 and N3. This confirms our findings based on the RF transmission studies discussed above (Figure 1).

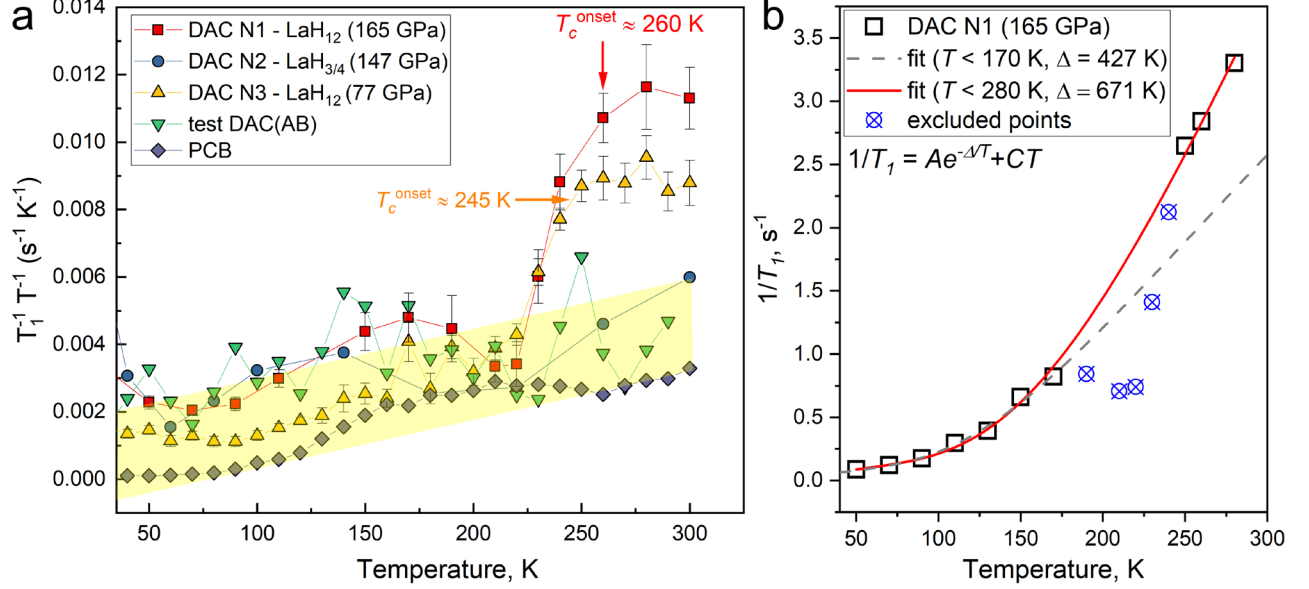


Figure 4. Nuclear spin-lattice relaxation rate $(T_1T)^{-1}$ of LaH_{12} (samples N1 and N3), and in other DACs and test samples. (a) Dependence of the relaxation time $1/T_1T$ in all studied samples on temperature. There is a pronounced drop in the relaxation rate in DACs N1 and N3 below 260 K and 245 K, respectively. This is associated with the presence of the LaH_{12} phase, which is absent in the other DACs and test samples. (b) Fitting of the temperature-dependent $1/T_1$ in DAC N1 at 165 GPa and 7 T. Here, “A” and “C” are fit parameters, $\Delta = \Delta(0)$ is the superconducting gap. The fit was performed for temperatures below 170 and 280 K, which is indicated by a gray dashed line and a red solid line, respectively.

Discussion

A key characteristic of type-I superconductors is the complete volume displacement of an applied external magnetic field in the superconducting state. By contrast, in type-II superconductors, in particular for granulated ones⁵³, the field penetrates the sample volume^{54,55,56}. As the NMR signal intensity is proportional to the penetrated sample volume, this facilitates NMR measurements of spectral characteristics and nuclear spin-lattice relaxation times even at temperatures below T_c (Figures 4a, b). The measured spin-lattice relaxation time in DAC N1 at 300 K is about 300 ms, and the product $TT_1 \approx 88$ sK. Comparing the low-temperature behavior of the spin-lattice relaxation in DACs N1 and N2, we note that the differences in TT_1 are small: we found $TT_1 = 573$ sK at 50 K in DAC N1, and 340 sK at 40 K in DAC N2. This is not surprising, given the fact that superconducting phases yield only a very small contribution to the NMR signal at $T \ll T_c$. The ^1H signal at low temperatures is mainly due to the residual non-superconducting hydrogen-containing compounds.

As Figures 4a,b and the Supporting Figure S25 show, there is a region of increased spin-lattice relaxation rate below 227 K, which can be associated with either the LaH_{12} or residual NH_3BH_3 . Phenomenologically, this upturn feature in the $1/T_1$ vs T plot resembles the relaxation behavior of ^{27}Al NMR measurements, studied in the classical Hebel-Slichter^{25,26} and Redfield-Anderson²⁴ experiments (Supporting Figure S25a). In this scenario, the hump below $T_c^{50\%}$ for DAC N1 may be caused by the contribution of a Hebel-Slichter-type coherence peak, indicating the opening of the SC

gap and the appearance of narrow maxima in the density of electronic states $N(E)$. Since the dependence $1/T_1 \propto N(E)^2$ is quadratic, the presence of peaks in $N(E)$ leads to a decrease of T_1 (the Hebel-Slichter peak). If this increase in the relaxation rate is indeed related to such a coherence peak and not to the residual amount of NH_3BH_3 (Supporting Figures S10, S26), it would be a strong argument in favor of conventional electron-phonon pairing in lanthanum superhydrides^{57,58}.

However, we would like to emphasize another observation, based on our $1/T_1$ data. In many superconductors, antiferromagnetic fluctuations⁵⁹, as well as a strong electron-phonon interaction⁶⁰, may suppress a possible Hebel-Slichter peak. The synthesized LaH_{12} is expected to be a superconductor in the strong coupling limit. Therefore, a most striking result can be obtained from fitting the temperature dependence of $1/T_1$ below T_c , allowing to determine the superconducting gap of LaH_{12} at 165 GPa. As shown in Figure 4b (and Figure S32), fitting the $1/T_1$ data for different temperature regimes leads to a rough estimate of the superconducting gap $\Delta(0)$ between about 427 and 671 K (36.8 to 57.8 meV), and $R_\Delta = 2\Delta(0)/k_B T_c$ of about 3.76 to 5.16, in qualitative agreement with the strong electron-phonon coupling extension of the BCS theory proposed by Migdal and Eliashberg^{61,62}.

The onset temperature of the superconducting transition in LaH_{12} deserves a separate discussion. Despite the fact that even in pure $Fm\bar{3}m\text{-LaH}_{10}$ in the absence of a magnetic field, the critical temperature T_c^{onset} does not exceed ≈ 250 K, in our experiment, an unusual behavior of the NMR spectra and $1/T_1 T$ is observed right above 260 K at a field of 7 T. Considering a typical value of the derivative $dB_{c2}/dT|_{T=T_c} \approx -1$ T/K for superhydrides^{63,64}, we estimate that, in the absence of magnetic field, superconductivity in the DAC N1 sets in already around 267 K, which is significantly higher than the onset transition observed in transport R - T measurements². Thus, the results of our NMR study in magnetic fields of 4 and 7 T agree well with the RF transmission measurements in the absence of magnetic field (Figure 1).

Measurements of the electrical transport are limited to the current path of least resistance. By contrast, the RF method senses the full bulk of the sample. Hence, differences in transition onset temperatures and feature weights detected by those techniques are a natural consequence. Once superconductivity sets in, the resistance drops to zero and any information below that transition is hidden. In inhomogeneous granular superconductors consisting of multiple phases with varying T_c , may be sensed a series-connected normal-metallic and superconducting resistances. Hence, step-like transitions with non-zero signatures may be detected. Indeed, such features have been noted previously in La-H^{3,41,43} and La-Sc-H systems¹² at temperatures much higher than 250 K. It is interesting to note that similar anomalies were also observed in the high-frequency AC susceptibility measurements of $\text{LaH}_{10\pm x}$ samples⁴².

Conclusions

Employing nuclear magnetic resonance spectroscopy and radio-frequency transmission measurements, we studied five samples of lanthanum hydrides, including two crystal modifications of LaH_{12} , LaH_{9+x} , tetragonal LaH_4 , and LaH_3 , at various pressures from 19 to 165 GPa in magnetic fields of 0, 4, and 7 T. The superconducting transition in the newly discovered $P6\text{-LaH}_{12}$ is characterized by a strong suppression of the ^1H NMR signal intensity below ~ 260 K in a magnetic field of 7 T. It is, furthermore, accompanied by a pronounced change in all NMR characteristics, including the spin-lattice relaxation rate $1/T_1 T$, which exponentially decreases at temperatures below T_c . Our estimate of the superconducting gap in LaH_{12} gives a $\Delta(0)$ of about 427 to 671 K (36.8 to 57.8 meV), and $R_\Delta = 2\Delta(0)/k_B T_c$ of about 3.76 to 5.16, in accordance with the strong-coupling scenario in lanthanum superhydrides.

We support these observations by additional radio-frequency transmission experiments on the same DAC in a transformer configuration, where the Lenz lenses act as primary and secondary coils. The transmission amplitude exhibits abrupt changes, already setting in at about 267 ± 5 K (at zero field). Surprisingly, the La-H system contains phases with significantly higher T_c than what was

previously reported on the basis of electrical transport measurements. In both studied samples, DACs N1 and N3, the detected changes in the NMR signal frequency, shape, width and, most importantly, the spin-lattice relaxation rate $1/T_1T$, start about 15-20 K above the zero-field onset T_c of the canonical LaH₁₀, determined by means of transport measurements.

Acknowledgments

D. S. and D. Z. thank the National Natural Science Foundation of China (NSFC, grant No. 12350410354) and Beijing Natural Science Foundation (grant No. IS23017) for the support of this research. D. Z. thanks the China Postdoctoral Science Foundation (No. 2023M740204) and the Fundamental Research Funds for the Central Universities for support of this research. This work was supported by the National Key Research and Development Program of China (grant 2023YFA1608900, subproject 2023YFA1608903). V.V.S. acknowledges the financial support from Shanghai Science and Technology Committee, China (No. 22JC1410300) and Shanghai Key Laboratory of Materials Frontier Research in Extreme Environments, China (No. 22dz2260800). We express our gratitude to Dr. Fuyang Liu, Dr. Yanping Yang and Dr. Hongliang Dong from Beijing and Shanghai HPSTAR for their help with the Ga FIB ion etching and magnetron sputtering of Al₂O₃, respectively. We also thank Dr. Thomas Meier (HPSTAR, Beijing) for technical support and drawing our attention to the NMR research using diamond anvil cells. We thank Prof. Yang Ding's group, especially Dr. Jianbo Zhang, at HPSTAR, Beijing, for allowing us to use the Raman spectrometer and the magnetron sputtering system. We would like to express our gratitude to Dr. Liuxiang Yang (HPSTAR, Beijing) for the laser heating of our samples. We thank Dr. Xiaoli Huang (Jilin University) and Dr. Liling Sun (HPSTAR, Beijing) for assistance with X-ray diffraction studies at the Shanghai synchrotron research facility. We also express our gratitude to the teams of the high-pressure stations ID27 (ESRF) and BL15U1 (SSRF) for their help in the XRD investigations. We acknowledge support from the Deutsche Forschungsgemeinschaft (DFG) through SFB 1143 (Project No. 247310070) and the Würzburg-Dresden Cluster of Excellence on Complexity and Topology in Quantum Matter - ct.qmat (EXC 2147, Project No. 390858490), as well as the support of the HLD at HZDR, member of the European Magnetic Field Laboratory (EMFL).

References

- 1 Drozdov, A. P., Eremets, M. I., Troyan, I. A., Ksenofontov, V. & Shylin, S. I. Conventional superconductivity at 203 kelvin at high pressures in the sulfur hydride system. *Nature* **525**, 73-76, doi:10.1038/nature14964 (2015).
- 2 Drozdov, A. P. *et al.* Superconductivity at 250 K in lanthanum hydride under high pressures. *Nature* **569**, 528-531, doi:10.1038/s41586-019-1201-8 (2019).
- 3 Somayazulu, M. *et al.* Evidence for Superconductivity above 260 K in Lanthanum Superhydride at Megabar Pressures. *Phys. Rev. Lett.* **122**, 027001, doi:10.1103/PhysRevLett.122.027001 (2019).
- 4 Semenok, D. V. *et al.* Superconductivity at 161 K in thorium hydride ThH₁₀: Synthesis and properties. *Mater. Today* **33**, 36-44, doi:10.1016/j.mattod.2019.10.005 (2020).
- 5 Troyan, I. A. *et al.* Synthesis and Superconductivity of Yttrium Hexahydride Im-3m-YH₆. *arXiv:1908.01534v1* (2019).
- 6 Kong, P. P. *et al.* Superconductivity up to 243 K in yttrium hydrides under high pressure. *arXiv:1909.10482*, doi:1909.10482 (2019).
- 7 Chen, W. *et al.* High-Temperature Superconducting Phases in Cerium Superhydride with a T_c up to 115 K below a Pressure of 1 Megabar. *Phys. Rev. Lett.* **127**, 117001, doi:10.1103/PhysRevLett.127.117001 (2021).
- 8 Troyan, I. A. *et al.* High-temperature superconductivity in hydrides. *Phys. Usp.* **65**, 748-761, doi:10.3367/UFNe.2021.05.039187 (2022).
- 9 Semenok, D. *Computational design of new superconducting materials and their targeted experimental synthesis* Doctoral program in materials science and engineering thesis thesis,

- Skoltech, (2022).
- 10 Semenok, D. V. *et al.* Observation of the Josephson effect in superhydrides: DC SQUID based on (La, Ce) H₁₀ with operating temperature of 179 K. *arXiv:2404.09199* (2024).
- 11 Dmitrii V. Semenok, A. V. S., Di Zhou, Oleg A. Sobolevskiy, Toni Helm, Sven Luther, Vladimir M. Pudalov, Ivan A. Troyan, Viktor V. Struzhkin. Superconducting memory and trapped magnetic flux in ternary lanthanum polyhydrides. *arXiv:2410.08730* (2024).
- 12 Semenok, D. V. *et al.* Ternary superhydrides under pressure of Anderson's theorem: Near-record superconductivity in (La, Sc) H₁₂. *arXiv:2408.07477* (2024).
- 13 Aslandukova, A. *et al.* Diverse high-pressure chemistry in Y-NH₃BH₃ and Y-paraffin oil systems. *Sci. Adv.* **10**, ead15416, doi:doi:10.1126/sciadv.ad15416 (2024).
- 14 Laniel, D. *et al.* High-pressure synthesis of seven lanthanum hydrides with a significant variability of hydrogen content. *Nat. Commun.* **13**, 6987, doi:10.1038/s41467-022-34755-y (2022).
- 15 Semenok, D. V., Altshuler, B. L. & Yuzbashyan, E. A. Fundamental limits on the electron-phonon coupling and superconducting T_c . *arXiv:2407.12922* (2024).
- 16 Sakakibara, T., Goto, T. & Miura, N. Contactless transport measurement of metals in pulsed high magnetic fields. *Review of Scientific Instruments* **60**, 444-449, doi:10.1063/1.1140398 (1989).
- 17 Timofeev, Y. A., Struzhkin, V. V., Hemley, R. J., Mao, H.-k. & Gregoryanz, E. A. Improved techniques for measurement of superconductivity in diamond anvil cells by magnetic susceptibility. *Rev. Sci. Instrum.* **73**, 371-377, doi:10.1063/1.1431257 (2002).
- 18 Meier, T. *et al.* In situ high-pressure nuclear magnetic resonance crystallography in one and two dimensions. *Matter and Radiation at Extremes* **6**, doi:10.1063/5.0065879 (2021).
- 19 Meier, T. *et al.* In-situ High Pressure Nuclear Magnetic Resonance Crystallography. *arXiv:2108.05506* (2021).
- 20 Günther, H. *NMR Spectroscopy: Basic Principles, Concepts and Applications in Chemistry 3rd Edition.* (John Wiley & Sons, 2013).
- 21 Rabi, I. I., Zacharias, J. R., Millman, S. & Kusch, P. A New Method of Measuring Nuclear Magnetic Moment. *Phys. Rev.* **53**, 318-318, doi:10.1103/PhysRev.53.318 (1938).
- 22 Müller, K. & Geppi, M. *Solid State NMR: Principles, Methods, and Applications.* (John Wiley & Sons, 2021).
- 23 Cooper, L. N. Microscopic Quantum Interference Effects in the Theory of Superconductivity. (1972).
- 24 Anderson, A. G. & Redfield, A. G. Nuclear Spin-Lattice Relaxation in Metals. *Phys. Rev.* **116**, 583-591, doi:10.1103/PhysRev.116.583 (1959).
- 25 Hebel, L. C. & Slichter, C. P. Nuclear relaxation in superconducting aluminum. *Phys. Rev.* **107**, 901, doi:10.1103/PhysRev.107.901 (1957).
- 26 Hebel, L. C. & Slichter, C. P. Nuclear spin relaxation in normal and superconducting aluminum. *Phys. Rev.* **113**, 1504, doi:10.1103/PhysRev.113.1504 (1959).
- 27 Knight, W. D. Nuclear Magnetic Resonance Shift in Metals. *Phys. Rev.* **76**, 1259-1260, doi:10.1103/PhysRev.76.1259.2 (1949).
- 28 F Smith, D. & P Slichter, C. *The study of mechanisms of superconductivity by NMR relaxation.* (2006).
- 29 Korringa, J. Nuclear magnetic relaxation and resonance line shift in metals. *Physica* **16**, 601-610, doi:[https://doi.org/10.1016/0031-8914\(50\)90105-4](https://doi.org/10.1016/0031-8914(50)90105-4) (1950).
- 30 Meier, T. *et al.* Magnetic flux tailoring through Lenz lenses for ultrasmall samples: A new pathway to high-pressure nuclear magnetic resonance. *Sci. Adv.* **3**, eaao5242, doi:10.1126/sciadv.aao5242 (2017).
- 31 Fu, Y. *et al.* Trace element detection in anhydrous minerals by micro-scale quantitative nuclear magnetic resonance spectroscopy. *Nat. Commun.* **15**, 7293, doi:10.1038/s41467-024-51131-0 (2024).
- 32 Meier, T. *et al.* Pressure-induced hydrogen-hydrogen interaction in metallic FeH revealed by NMR. *Phys. Rev. X* **9**, 031008, doi:10.1103/PhysRevX.9.031008 (2019).
- 33 Meier, T. *et al.* Proton mobility in metallic copper hydride from high-pressure nuclear

- magnetic resonance. *Phys. Rev. B* **102**, 165109, doi:10.1103/PhysRevB.102.165109 (2020).
- 34 Meier, T. *et al.* Nuclear spin coupling crossover in dense molecular hydrogen. *Nat. Commun.* **11**, 6334, doi:10.1038/s41467-020-19927-y (2020).
- 35 Yang, M. *et al.* Hexagonal to Monoclinic Phase Transition in Dense Hydrogen Phase III Detected by High-Pressure NMR. *arXiv:2407.19368* (2024).
- 36 Shitaokoshi, T., Kawachi, S., Nomura, T., Balakirev, F. F. & Kohama, Y. Radio frequency electrical resistance measurement under destructive pulsed magnetic fields. *Review of Scientific Instruments* **94**, doi:10.1063/5.0165680 (2023).
- 37 Spengler, N., While, P. T., Meissner, M. V., Wallrabe, U. & Korvink, J. G. Magnetic Lenz lenses improve the limit-of-detection in nuclear magnetic resonance. *PLOS ONE* **12**, e0182779, doi:10.1371/journal.pone.0182779 (2017).
- 38 Sun, D. *et al.* High-temperature superconductivity on the verge of a structural instability in lanthanum superhydride. *Nat. Commun.* **12**, 6863, doi:10.1038/s41467-021-26706-w (2021).
- 39 Kruglov, I. A. *et al.* Superconductivity of LaH₁₀ and LaH₁₆ polyhydrides. *Phys. Rev. B* **101**, 024508, doi:10.1103/PhysRevB.101.024508 (2020).
- 40 Kantor, I. *et al.* BX90: A new diamond anvil cell design for X-ray diffraction and optical measurements. *Review of Scientific Instruments* **83**, 125102, doi:10.1063/1.4768541 (2012).
- 41 Grockowiak, A. D. *et al.* Hot Hydride Superconductivity Above 550 K. *Frontiers in Electronic Materials* **2**, doi:10.3389/femat.2022.837651 (2022).
- 42 Struzhkin, V. *et al.* Superconductivity in La and Y hydrides: Remaining questions to experiment and theory. *Matter Radiat. Extremes* **5**, 028201, doi:10.1063/1.5128736 (2020).
- 43 Wu, Y. L. *et al.* Ultrafast dynamics evidence of strong coupling superconductivity in LaH_{10±δ}. *Nature communications* **15**, 9683, doi:10.1038/s41467-024-53103-w (2024).
- 44 Macrae, C. F. *et al.* Mercury 4.0: from visualization to analysis, design and prediction. *J. Appl. Crystallogr.* **53**, 226-235, doi:10.1107/S1600576719014092 (2020).
- 45 Hrubciak, R., Smith, J. S. & Shen, G. Multimode scanning X-ray diffraction microscopy for diamond anvil cell experiments. *Review of Scientific Instruments* **90**, 025109, doi:10.1063/1.5057518 (2019).
- 46 Kuzovnikov, M. A. in *The 27th AIRAPT International Conference on High Pressure and Technology* (Rio de Janeiro, Brasil, 2019).
- 47 Kuzovnikov, M. A. *et al.* in *57th EHPRG Meeting on High Pressure Science and Technology* (Prague, Czech Republic, 2019).
- 48 Kuzovnikov, M. A. in *XXXVI Fortov International Conference on Interaction of Intense Energy Fluxes with Matter (ELBRUS 2021)* (ELBRUS, 2021).
- 49 Bi, J. *et al.* Stabilization of superconductive La-Y alloy superhydride with *T_c* above 90 K at megabar pressure. *Mater. Today Phys.*, 100840, doi:<https://doi.org/10.1016/j.mtphys.2022.100840> (2022).
- 50 Chen, W. *et al.* Enhancement of superconducting critical temperature realized in La-Ce-H system at moderate pressures. *Nat. Commun.* **14**, 2660, doi:10.1038/s41467-023-38254-6 (2023).
- 51 Gunaydin-Sen, O., Achey, R., Dalal, N. S., Stowe, A. & Autrey, T. High Resolution ¹⁵N NMR of the 225 K Phase Transition of Ammonia Borane (NH₃BH₃): Mixed Order-Disorder and Displacive Behavior. *The Journal of Physical Chemistry B* **111**, 677-681, doi:10.1021/jp0649347 (2007).
- 52 COMSOL Multiphysics v. 6.0.
- 53 Semenok, D. V. *et al.* Superconducting memory and trapped magnetic flux in ternary lanthanum polyhydrides. *Materials Today Physics*, 101595, doi:<https://doi.org/10.1016/j.mtphys.2024.101595> (2024).
- 54 Abrikosov, A. A. The magnetic properties of superconducting alloys. *J. Phys. Chem. Solids* **2**, 199-208, doi:[https://doi.org/10.1016/0022-3697\(57\)90083-5](https://doi.org/10.1016/0022-3697(57)90083-5) (1957).
- 55 Sadakov, A. V. *et al.* Vortex Phase Dynamics in Yttrium Superhydride YH₆ at Megabar Pressures. *J. Phys. Chem. Lett.* **14**, 6666-6671, doi:10.1021/acs.jpcclett.3c01577 (2023).
- 56 Sadakov, A. V. *et al.* Quasi Two-dimensional Vortex Matter in ThH₁₀ Superhydride. *arXiv:2311.01318* (2023).

- 57 Minkov, V. S., Ksenofontov, V., Bud'ko, S. L., Talantsev, E. F. & Erements, M. I. Magnetic flux trapping in hydrogen-rich high-temperature superconductors. *Nat. Phys.* **19**, 1293–1300, doi:10.1038/s41567-023-02089-1 (2023).
- 58 Erements, M. I., Minkov, V. S., Drozdov, A. P. & Kong, P. P. The characterization of superconductivity under high pressure. *Nat. Mater.* **23**, 26-27, doi:10.1038/s41563-023-01769-w (2024).
- 59 Cavanagh, D. C. & Powell, B. J. Fate of the Hebel-Slichter peak in superconductors with strong antiferromagnetic fluctuations. *Physical Review Research* **3**, 013241, doi:10.1103/PhysRevResearch.3.013241 (2021).
- 60 Akis, R. & Carbotte, J. P. Damping effects on NMR in superconductors. *Solid State Communications* **78**, 393-396, doi:[https://doi.org/10.1016/0038-1098\(91\)90691-N](https://doi.org/10.1016/0038-1098(91)90691-N) (1991).
- 61 Migdal, A. B. Interaction between electrons and lattice vibrations in a normal metal. *Sov. Phys. JETP* **7**, 996 (1958).
- 62 Eliashberg, G. M. Interactions between electrons and lattice vibrations in a superconductor. *Sov. Phys. JETP* **11**, 696-709 (1960).
- 63 Semenok, D. *et al.* Evidence for Pseudogap Phase in Cerium Superhydrides: CeH₁₀ and CeH₉. *arXiv:2307.11742v2* (2023).
- 64 Semenok, D. V. *et al.* Effect of Magnetic Impurities on Superconductivity in LaH₁₀. *Adv. Mater.* **34**, 2204038, doi:<https://doi.org/10.1002/adma.202204038> (2022).